Lawrence Berkeley National Laboratory

Title
Transparent and conductive indium doped cadmium oxide thin films prepared by pulsed filtered cathodic arc deposition

Author
Zhu, Yuankun

Publication Date
2013-01-15

DOI
10.1016/j.apsusc.2012.11.096

Peer reviewed

Accepted for publication on 9 November 2012,
Published on-line on 15 January 2013, in
Applied Surface Science 265 (2013) 738-744
http://dx.doi.org/10.1016/j.apsusc.2012.11.096

Transparent and conductive indium doped cadmium oxide thin films prepared by pulsed filtered cathodic arc deposition

Yuankun Zhu [a, b], **Rueben J. Mendelsberg** [b, c], **Jiaqi Zhu** [a *], **Jiecai Han** [a], **André Anders** [b]

[a] *Center for Composite Materials and Structures, Harbin Institute of Technology, Harbin 150080, P. R. China*

[b] *Plasma Applications Group, Lawrence Berkeley National Laboratory, Berkeley, California, 94720*

[c] *Molecular Foundry, Lawrence Berkeley National Laboratory, Berkeley, California, 94720*

* Corresponding author:

Jiaqi Zhu
Tel. / Fax: +86-451-86417970;
Email: zhujq@hit.edu.cn
YiKuang Street 2, Post-box 3010,
Harbin 150080, P.R. China

ACKNOWLEDGEMENTS

The authors would like to thank K.M. Yu and S.H.N. Lim for their contributions to this work. Research was supported in-part by the LDRD Program of Lawrence Berkeley National Laboratory, in-part by the Assistant Secretary for Energy Efficiency and Renewable Energy, Office of Building Technology, of the U.S. Department of Energy under U.S. Department of Energy Contract No. DE-AC02-05CH11231. Portions of this work were performed as a user project at the LBNL Molecular Foundry, which is supported by the Office of Science, Office of Basic Energy Sciences, under the same contract. Additional support was provided by the National Natural Science Foundation of China (Grant No.51072039 and 50972031), and the Ph.D. Programs Foundation of the Ministry of Education of China (20112302110036).

Abstract

Indium doped cadmium oxide (CdO:In) films with different In concentrations were prepared on low-cost glass substrates by pulsed filtered cathodic arc deposition (PFCAD). It is shown that polycrystalline CdO:In films with smooth surface and dense structure are obtained. In-doping introduces extra electrons leading to remarkable improvements of electron mobility and conductivity, as well as improvement in the optical transmittance due to the Burstein–Moss effect. CdO:In films on glass substrates with thickness near 230 nm show low resistivity of 7.23×10^{-5} Ωcm, high electron mobility of 142 cm^2/Vs, and mean transmittance over 80% from 500-1250 nm (including the glass substrate). These high quality pulsed arc-grown CdO:In films are potentially suitable for high efficiency multi-junction solar cells that harvest a broad range of the solar spectrum.

Keywords: In doped cadmium oxide; pulsed filtered cathodic arc deposition; transparent conductors

1. Introduction

Transparent conducting oxides (TCOs) have attracted much attention due to their tremendous importance in optical and electrical applications such as displays, touch-screens, thin film solar cell technology and for transparent conducting electrodes in general [1, 2]. For solar cell applications, high mobility TCO contacts with a sheet resistance of <10 Ω/□ and an optical transmission >80% over the visible to near infrared wavelengths (bandgap >3 eV) can enhance the efficiency [3]. This is particularly effective for multi-junction solar cells which consist of different semiconductor stacks with appropriately matched bandgaps that are tuned to increase the spectral response over the entire solar spectrum [4]. Therefore, in addition to maintaining high conductivity, improving the visible to near infrared transparency of TCO films is of great importance for applications in high performance multi-junction solar cells.

Cadmium oxide (CdO) is a well-known transparent and conductive material with exceptional intrinsic electron mobility, nearly metallic conductivity, and high transparency in the near infrared (NIR) region. Though undoped CdO is not suitable for some TCO applications because of the relatively narrow bandgap and environmental issues [5], after appropriate bandgap widening, CdO-based materials could be widely used in high performance solar cells which already contain a large amount of Cd [6, 7]. It is known that the optical absorption edge can be considerably widened via a Burstein-Moss shift by increasing the electron concentration [8, 9]. Therefore, various dopants, including indium (In), tin (Sn), titanium (Ti), zinc (Zn), aluminum (Al), and fluorine (F), have been introduced into CdO to simultaneously increase the conductivity and widen the bandgap [10-18]. Among these doping elements, indium has been investigated in CdO since the two elements have very close ionic radii and both show excellent photoelectric properties [15, 19]. Furthermore, In-doping can favorably alter the CdO band structure by extensive mixing of In 5s and Cd 5s states, which lowers optical absorption by weakening the intraband transitions [12].

Doped and undoped CdO thin films have been prepared on various substrates by different film growth techniques. Impressive Hall mobility of 609 cm^2/Vs was reported for CdO films doped with 2.5% Sn (with resistivity of 2.38×10^{-5} Ωcm), which were deposited on single crystal MgO (111) substrates by pulsed laser deposition (PLD) [11]. However, on low-cost glass substrates, the mobility was only 27 cm^2/Vs. Similar to PLD, pulsed filtered cathodic arc deposition (PFCAD) produces a highly ionized flux of material and utilizes both the kinetic and potential energy of the arriving ions to grow high quality thin films [20]. Compared with PLD, PFCAD produces similar quality films but is easier to scale up and more cost effective, which is crucial for large-area applications. PFCAD has been demonstrated to be a technology suitable to make high quality aluminum doped zinc oxide (AZO) films at relatively low temperature [21]. The obtained optical and electrical parameters are comparable to or slightly better than the best films obtained by other methods such as magnetron sputtering (MS) and PLD [21, 22]. However, to the best of our knowledge, PFCAD has not been used to grow doped or undoped CdO thin films. The relatively low growth temperature, high reproducibility, and cost-efficiency of PFCAD make it a promising deposition technique for industrial applications with strict demands on material performance. In this work, we study the electrical, optical, and structural properties of indium doped cadmium oxide (ICO) thin films with different In concentrations prepared by PFCAD.

2. Experiment

ICO thin films with different In concentrations were prepared on borosilicate glass substrates by PFCAD. For comparison, undoped CdO films were also prepared at the same condition. Each deposition for a given growth condition was repeated three times in order to observe the reproducibility of the film growth and to provide an accurate estimate of the overall uncertainties. The repetition of those film growth experiments was done in a random order to minimize possible effects of any systematic drifts or uncertainties.

The plasma source utilized two cathode rods of 6.25 mm diameter each. Each cathode was enclosed by an alumina ceramic tube such that the cathode spots can operate only on the front surface [21]. Metallic cadmium (99.99% purity) and indium (99.99% purity) rods were used as the two cathodes. The cadmium and indium plasmas passed through a 90°-bend open coil electromagnetic filter to remove most of the macroparticles [23]. The concentration of indium in the films was controlled by adjusting the ratio of pulses on each of the two cathodes. A similar setup of the growth system for ICO film deposition can be seen in ref 22.

Borosilicate microscope glass slides were used as substrates. Before mounting them on the substrate holder, the glass substrates were gently cleaned using commercial glass detergent (Liquinox®) as discussed in earlier work [24]. The substrates were heated up to 220±10 ℃ using a 4-lamp radiative heater once the chamber was cryogenically pumped to a base pressure of about 5×10^{-6} Torr. When the substrate was hot, the base pressure was around $1{\sim}2\times10^{-5}$ Torr after the cryogenic pump was partially valved off. Pure oxygen was injected into the chamber with a flow rate of 46 SCCM using a mass flow controller (MKS Instruments). The growth pressure was set to 7 mTorr by controlling the pumping speed of the cryogenic pump through an adjustable gate valve. During film growth, arc pulses of 1 ms duration and amplitude of 780 A were delivered with a repetition rate of 1 pulse per second by a pulse-forming network [25]. For each growth, 1500 pulses in total were used. ICO thin films with In concentrations of 0%, 1.2±0.4%, 2.2±0.7%, 2.4±0.5%, 4.2±0.7%, and 9.1±1% (In:Cd, at. %) were prepared at 220 ℃ and 7 mTorr. For each growth condition, three samples were obtained with thickness in the range of 220~250 nm.

Film thickness was measured using step profilometry, and film composition was characterized by energy-dispersive X-ray spectroscopy (EDS, FEI Quanta 200FEG). Film surface morphology was studied with a Veeco MultiMode AFM in tapping mode and scanning electron microscope (Carl Zeiss Ultra

55-SEM). Film structure was investigated by a Bruker X-ray diffractometer equipped with an area detector. A LaB_6 powder diffraction standard was used to ensure calibration of the 2θ angle and to measure the instrumental broadening. Optical transmittance and reflectance measurements from 250-2500 nm were taken with a Perkin-Elmer Lambda 950 dual beam spectrophotometer equipped with the universal reflectance accessory. The electrical properties of the films were characterized at room temperature by Hall measurements in the Van der Pauw geometry using an Ecopia HMS-3000 system with a 0.6 T magnet.

3. Results

3.1 Film structure

Fig. 1 shows the surface morphologies of ICO films with different In concentrations characterized by SEM. The ICO films grown on glass substrates by PFCAD are uniform and densely packed. Smooth surface and featureless morphology of the undoped and doped CdO films are observed. The inconspicuous variation of the surface morphology with In doping is also observed with an atomic force microscope (AFM) as shown in Fig. 2. Uniformly distributed features with no pinholes or island structures are observed in all the ICO films. The root mean square (RMS) roughness (*Rq*) is less than 2 nm over a 1μm×1μm area for all the films. The pulsed arc-grown ICO films show roughness almost independent of In concentration. However, *Rq* scales with film thickness. A 2.2% ICO film (grown under the same conditions) with thickness of about 640 nm shows high *Rq* of about 3.15 nm and the 135 nm thick ICO film shows *Rq* of about 1.06 nm.

The XRD patterns of ICO thin films with different In concentrations are shown in Fig. 3. It is observed that all the ICO films are phase-pure with all XRD features assignable to cubic CdO. No In_2O_3 or other phases are observed, indicating that most of the In^{3+} substitutes the Cd^{2+} in the lattice instead of forming a new phase. Diverse growth orientations of the ICO films are clearly observed but there is no shifting of the peak positions. The preferential orientation of the ICO films varies with increasing In concentration and the relative intensity ratio of the (200) peak to the (220) peak (I_{200}/I_{220}) is shown in Table 1. The mean grain size (D) is calculated from the Scherrer equation using all of the diffraction peaks and shown in Table 1. To investigate the grain size carefully, the Hall-Williamson method which is used in some CdO papers is also utilized for grain size and microstrain calculation [18, 26]. The Hall-Williamson plot is not quite linear but indicates small compressive microstrain ($5\text{-}8\times10^{-3}$) and gives similar values of the grain size obtained from the Scherrer equation. Therefore, taking into account the uncertainties, the mean grain size is approximately constant with increasing In concentration.

3.2 Electrical properties

The resistivity and sheet resistance (RS) of ICO films with different In concentrations are shown in Fig. 4. As expected, In-doping decreases the resistivity and sheet resistance significantly. However, the resistivity and sheet resistance start to increase slightly at high In concentrations. For each condition, the resistivity of the as-grown ICO thin films is quite reproducible. With increasing In doping, the carrier concentration substantially increases, presumably due to In^{3+} ions substituted on Cd^{2+} sites. The Hall mobility initially increases significantly, and subsequently decreases with increasing In concentration. The electrical properties of ICO films with different In concentrations are listed in Table 2.

3.3 Optical properties

Highly transparent ICO films with a slight yellow tinge were obtained by PFCAD. The optical transmittance and reflectance of ICO/glass stacks with different In concentrations are shown in Fig. 5. The visible to near infrared transmittance improves significantly and the transparent range is extended with increasing In doping. Doping causes a shift in the bandgap absorption edges to shorter wavelength, moving from 460-500 nm in the undoped CdO films to 350-390 nm in the ICO films. Simultaneously, the plasma edge (λ_{RT}), evaluated by the intersection of the transmittance and reflectance, blue-shifts as shown in Table 1. From 500 nm to 1250 nm wavelength, the average transmittance of the ICO/glass stacks is over 80% and changes very slightly with increasing In concentration. In particular, the film with 1.2% In shows >80% transmittance for wavelengths as long as 1800 nm.

The optical bandgap of the ICO films is calculated using the fundamental absorption, which corresponds to electron excitation from the valance band to conduction band. The absorption coefficient (α) is calculated using the equation [27]:

$$\alpha = -\frac{1}{d}\ln[\frac{T}{(1-R)^2}]$$

where T is transmittance, R is reflectance, and d is film thickness. The absorption coefficient (α) and the incident photon energy ($h\nu$) are related by[18] :

$$(\alpha h\nu)^2 = A(h\nu - E_g)$$

where $h\nu$, A and E_g are the photon energy, a constant, and the optical band gap, respectively. The direct optical bandgap of ICO thin films with different In concentrations is shown in Fig. 6. As expected, the optical bandgap substantially increases with increasing In concentration as shown in Table 1. It should be pointed out here that the calculated optical bandgap is about 0.02~0.05eV smaller than that in Table 1 when the reflectance was neglected (i.e. R=0).

4. Discussions

As it is well known, the structural, electrical and optical properties of TCO films are dependent on the doping level. In this study, variation of film properties with increasing In concentration is observed. In Fig. 3, the diverse growth orientations of the ICO films are attributed to the amorphous glass surface introducing no energetic restrictions/growth templating [28]. The variation of the preferred orientation with increasing In concentration is likely due to the diffusion rate variation of Cd and O atoms induced by In doping [13]. Similar phenomena are also observed for the fluorine doped CdO films and PLD-grown ICO films [13, 29]. There is no significant shift of the diffraction peaks, indicating the lattice parameters are essentially invariant. This is surprising since In^{3+} has a smaller ionic radius (In^{3+} 0.94 Å compared to Cd^{2+} 1.09 Å) and the lattice parameter is expected to shrink with increasing In concentration. Lattice shrinkage and a decrease in grain size of ICO films prepared by other techniques have been observed [14, 30]. According to Table 1, it is known that the film crystalline quality does not deteriorate significantly with increasing In concentration.

The low electrical resistivity of the undoped CdO thin films is associated with its native defects of oxygen vacancies and cadmium interstitials [31]. The variation of the Hall mobility with increasing In concentration can be explained as follows: Two main scattering mechanisms including grain boundary scattering and ionized impurity scattering exist in the doped CdO thin films. At low doping level, the grain boundary scattering is predominant [32]. Indium doping lowers the potential barrier of grain boundaries due to screening induced by the free electrons [11]. Therefore, the carrier mobility increases for low In concentrations. As the In doping level is further increased, the relatively high density of ionized In centers counteract the charge carrier movement resulting in the increase of charge carrier scattering, which leads to the decrease of mobility as shown in Fig. 3.

Table 2 shows the electrical properties of the pulsed arc-grown ICO films compared to values reported for several other growth techniques. Except for the optimized PLD-grown films [19], the electrical properties of films prepared by PFCAD in this study are typically better than those of ICO films prepared by other techniques on glass or even on single crystalline MgO substrates [10, 12, 14, 30, 33-36]. Though the as-deposited films in this study show a little higher resistivity than that of the optimized PLD-grown films, comparable mobility with a higher near infrared transmittance and a much wider transparent range are observed, which is of special interest to multi-junction solar cells.

The visible to solar-infrared transmittance of the ICO films improves significantly with In doping. Blue shift of the bandgap absorption edge is observed and is due to the increase of carrier concentration due to the Burstein–Moss effect [8]. Assuming the Fermi surface is spherical, the following equation was derived for the Burstein-Moss effect [9, 37]:

$$E_g = E_g^0 + \Delta E_g^{BM}$$

The Burstein-Moss shift ΔE_g^{BM} is given by

$$\Delta E_g^{BM} = \frac{\hbar^2}{2m_{vc}^*}(3\pi^2 n_e)^{2/3}$$

where E_g^0, m_{vc}^*, n_e are the intrinsic bandgap of an undoped semiconductor, the reduced effective mass, and carrier concentration, respectively. In Fig. 7, the bandgap of the doped CdO films is plotted against two-thirds power of carrier concentrations ($n_e^{2/3}$). The intrinsic bandgap of the undoped CdO (E_g^0) is evaluated to be 2.61±0.03 eV, which is similar to the measured value of 2.65±0.02 eV of the three undoped CdO films. The reduced effective mass is calculated to be 0.56-0.65 m_e, which is higher than that of 0.11-0.28 m_e of the undoped CdO films and close to that of ITO [27, 38]. The high calculated effective mass is owing to ignoring the bandgap shrinkage effect which is due to the electron-dopant interaction, electron-electron Coulomb and exchange interactions within the conduction band [37]. Dou *et al.* calculated the effective mass of 0.8~2.3 at.% ICO materials with carrier concentration about 5.8~9.8×10^{20} cm^{-3} to be about 0.31~0.43 m_e by accounting for the bandgap shrinkage effects [39]. In this study, the experimental data are in approximate agreement with the theoretical prediction. Therefore, the bandgap widening can be reasonably explained by the Burstein–Moss effect overcoming the shrinkage caused by many-body effects.

During film growth, cathodic arcs produce dense plasma with moderately energetic ions that are beneficial in terms of film quality. The average kinetic energy of Cd ions for a vacuum arc is 26 eV with significant amounts of ions in the tail of the energy distribution function up to 1.5 times the average value [40, 41]. Collisions of the Cd ions with oxygen will provide excitation, ionization, and kinetic energy to oxygen, which promotes oxidation of the Cd and formation of high quality CdO. The deposition process is "energetic" with contributions of both kinetic and potential energy to the film growth process [21, 42]. Significant low-energy ion bombardment during growth enhances the atom mobility without causing damage to the lattice, resulting in high quality films. Therefore, ICO films with excellent structural, electrical, and optical properties are achieved.

5. Conclusion

High quality ICO thin films were prepared on low-cost glass substrates by PFCAD. The pulsed arc-grown films show excellent reproducibility of film thickness, structural, electrical, and optical properties. The 230 nm thick ICO films show low resistivity of 7.2×10^{-5} Ωcm, sheet resistance as low as 3.1 Ω/□, and electron mobility as high as 142 cm^2/Vs while maintaining an average transmittance over 80% from 500 nm to at least 1250 nm. With In doping, the bandgap absorption edge shifts considerably toward shorter wavelength due to the Burstein–Moss effect, improving the visible to near infrared optical transmittance. With In doping of 1.2 at. %, the electrical and optical properties are remarkably improved without detrimentally affecting the film structure or surface morphology. The relatively high electron mobility of CdO compared to other TCOs ensures that high conductivity material is obtained with moderate In doping. Thus, arc-grown CdO:In would make for high performance TCO contacts for high efficiency multi-junction solar cells made from Cd-based absorbers that are designed to harvest photons of the entire solar spectrum. The relatively low growth temperature, high reproducibility, and the potential of arc deposition to be scaled to large area, make ICO films grown by PFCAD a promising material for industrial applications where high performance TCOs are required and the presence of Cd is acceptable since Cd or similarly hazardous material are already present.

References

[1] H. Kim, C.M. Gilmore, A. Pique, J.S. Horwitz, H. Mattoussi, H. Murata, Z.H. Kafafi, D.B. Chrisey, Electrical, optical, and structural properties of indium–tin–oxide thin films for organic light-emitting devices, J. Appl. Phys. 86 (1999) 6451-6461.

[2] T. Minami, H. Tanaka, T. Shimakawa, T. Miyata, H. Sato, High-Efficiency oxide heterojunction solar cells using Cu_2O Sheets, Jpn. J. Appl. Phys. 43 (2004) L917-L919.

[3] S. Calnan, A.N. Tiwari, High mobility transparent conducting oxides for thin film solar cells, Thin solid films 518 (2010) 1839-1849.

[4] T.J. Coutts, J.S. Ward, D.L. Young, K.A. Emery, T.A. Gessert, R. Noufi, Critical issues in the design of polycrystalline, thin-film tandem solar cells, Prog. Photovoltaics Res. Appl. 11 (2003) 359-375.

[5] N. Ueda, H. Maeda, H. Hosono, H. Kawazoe, Band-gap widening of CdO thin films, J. Appl. Phys. 84 (1998) 6174-6177.

[6] M.A. Contreras, B. Egaas, K. Ramanathan, J. Hiltner, A. Swartzlander, F. Hasoon, R. Noufi, Progress toward 20% efficiency in Cu(In,Ca)Se_2 polycrystalline thin-film solar cells, Prog. Photovoltaics 7 (1999) 311-316.

[7] O. Niitsoo, S.K. Sarkar, C. Pejoux, S. Ruhle, D. Cahen, G. Hodes, Chemical bath deposited CdS/CdSe-sensitized porous TiO_2 solar cells, J. Photochem. Photobiol., A 181 (2006) 306-313.

[8] E. Burstein, Anomalous optical absorption limit in InSb, Phys. Rev. 93 (1954) 632-633.

[9] I. Hamberg, C.G. Granqvist, K.F. Berggren, B.E. Sernelius, L. Engström, Band-gap widening in heavily Sn-doped In_2O_3, Phys. Rev. B 30 (1984) 3240-3249.

[10] R. Kumaravel, K. Ramamurthi, V. Krishnakumar, Effect of indium doping in CdO thin films prepared by spray pyrolysis technique, J. Phys. Chem. Solids 71 (2010) 1545-1549.

[11] M. Yan, M. Lane, C.R. Kannewurf, R.P.H. Chang, Highly conductive epitaxial CdO thin films prepared by pulsed laser deposition, Appl. Phys. Lett. 78 (2001) 2342-2344.

[12] A. Wang, Indium-cadmium-oxide films having exceptional electrical conductivity and optical transparency: Clues for optimizing transparent conductors, Proc. Natl. Acad. Sci. 98 (2001) 7113-7116.

[13] B.J. Zheng, J.S. Lian, L. Zhao, Q. Jiang, Optical and electrical properties of In-doped CdO thin films fabricated by pulse laser deposition, Appl. Surf. Sci. 256 (2010) 2910-2914.

[14] M.A. Flores, R. Castanedo, G. Torres, O. Zelaya, Optical, electrical and structural properties of indium-doped cadmium oxide films obtained by the sol-gel technique, Sol. Energy Mater. Sol. Cells 93 (2009) 28-32.

[15] A.J. Freeman, K.R. Poeppelmeier, T.O. Mason, R.P.H. Chang, T.J. Marks, Chemical and thin-film strategies for new transparent conducting oxides, MRS Bull. 25 (2000) 45-51.

[16] R.K. Gupta, K. Ghosh, R. Patel, P.K. Kahol, Highly conducting and transparent Ti-doped CdO films by pulsed laser deposition, Appl. Surf. Sci. 255 (2009) 6252-6255.

[17] R. Deokate, S. Pawar, A. Moholkar, V. Sawant, C. Pawar, C. Bhosale, K. Rajpure, Spray deposition of highly transparent fluorine doped cadmium oxide thin films, Appl. Surf. Sci. 254 (2008) 2187-2195.

[18] B. Saha, S. Das, K.K. Chattopadhyay, Electrical and optical properties of Al doped cadmium oxide thin films deposited by radio frequency magnetron sputtering, Sol. Energy Mater. Sol. Cells 91 (2007) 1692-1697.

[19] R.K. Gupta, K. Ghosh, R. Patel, S.R. Mishra, P.K. Kahol, Structural, optical and electrical properties of In doped CdO thin films for optoelectronic applications, Mater. Lett. 62 (2008) 3373-3375.

[20] A. Anders, Cathodic Arcs: From Fractal Spots to Energetic Condensation, Springer, New York, 2008.
[21] A. Anders, S.H.N. Lim, K.M. Yu, J. Andersson, J. Rosén, M. McFarland, J. Brown, High quality ZnO:Al transparent conducting oxide films synthesized by pulsed filtered cathodic arc deposition, Thin solid films 518 (2010) 3313-3319.
[22] K. Ellmer, Magnetron sputtering of transparent conductive zinc oxide: relation between the sputtering parameters and the electronic properties, J. Phys. D: Appl. Phys. 33 (2000) R17-R32.
[23] A. Anders, Approaches to rid cathodic arc plasmas of macro- and nanoparticles: a review, Surf. Coat. Technol. 120 (1999) 319-330.
[24] R.J. Mendelsberg, S.H.N. Lim, Y.K. Zhu, J. Wallig, D.J. Milliron, A. Anders, Achieving high mobility ZnO : Al at very high growth rates by dc filtered cathodic arc deposition, J. Phys. D: Appl. Phys. 44 (2011) 232003-1-232003-5.
[25] A. Anders, R.A. MacGill, T.A. McVeigh, Efficient, compact power supply for repetitively pulsed, "triggerless" cathodic arcs, Rev. Sci. Instrum. 70 (1999) 4532-4535.
[26] R. Maity, K.K. Chattopadhyay, Synthesis and characterization of aluminum-doped CdO thin films by sol–gel process, Sol. Energy Mater. Sol. Cells 90 (2006) 597-606.
[27] X. Li, D.L. Young, H. Moutinho, Y. Yan, C. Narayanswamy, T.A. Gessert, T.J. Coutts, Properties of CdO Thin Films Produced by Chemical Vapor Deposition, Electrochem. Solid-State Lett. 4 (2001) C43-C46.
[28] L. Wang, Y. Yang, S. Jin, T.J. Marks, MgO(100) template layer for CdO thin film growth: Strategies to enhance microstructural crystallinity and charge carrier mobility, Appl. Phys. Lett. 88 (2006) 162115-1-162115-3.
[29] M. Kul, A.S. Aybek, E. Turan, M. Zor, S. Irmak, Effects of fluorine doping on the structural properties of the CdO films deposited by ultrasonic spray pyrolysis, Sol. Energy Mater. Sol. Cells 91 (2007) 1927-1933.
[30] Y. Yang, S. Jin, J.E. Medvedeva, J.R. Ireland, A.W. Metz, J. Ni, M.C. Hersam, A.J. Freeman, T.J. Marks, CdO as the archetypical transparent conducting oxide systematic of dopant ionic radius and electronic structure effects on charge transport and band structure, J. Am. Chem. Soc. 127 (2005) 8796-8804.
[31] Y. Dou, T. Fishlock, R.G. Egdell, Band-gap shrinkage in n-type-doped CdO probed by photoemission spectroscopy, Phys. Rev. B 55 (1997) R13381-R13384.
[32] S.K. Vasheghani Farahani, T.D. Veal, P.D.C. King, J. Zuniga-Perez, V. Munoz-Sanjose, C.F. McConville, Electron mobility in CdO films, J. Appl. Phys. 109 (2011) 073712-1-073712-5.
[33] P.M. Babu, G.V. Rao, S. Uthanna, Transparent conductive cadmium indate thin films prepared by dc magnetron sputtering, Mater. Chem. Phys. 78 (2002) 208-213.
[34] X. Wu, T.J. Coutts, W.P. Mulligan, Properties of transparent conducting oxides formed from CdO and ZnO alloyed with SnO_2 and In_2O_3, J. Vac. Sci. Technol. A 15 (1997) 1057-1062.
[35] T.J. Coutts, X. Wu, W.P. Mulligan, High performance transparent conducting films of cadmium indate prepared by RF sputtering, Mat. Res. Soc. Symp. Proc. 426 (1996) 479-489.
[36] S. Jin, Y. Yang, J.E. Medvedeva, L. Wang, S. Li, N. Cortes, J.R. Ireland, A.W. Metz, J. Ni, M.C. Hersam, A.J. Freeman, T.J. Marks, Tuning the properties of transparent oxide conductors dopant ion size and electronic structure effects on CdO-based transparent conducting oxides Ga- and In-doped CdO thin films grown by MOCVD, Chem. Mater. 20 (2008) 220-230.
[37] B.E. Sernelius, K.F. Berggren, Z.C. Jin, I. Hamberg, C.G. Granqvist, Band-gap tailoring of ZnO by

means of heavy Al doping, Phys. Rev. B 37 (1988) 10244-10248.
[38] R. Zhuo, H. Feng, D. Yan, J. Chen, J. Feng, J. Liu, P. Yan, Rapid growth and photoluminescence properties of doped ZnS one-dimensional nanostructures, J. Cryst. Growth 310 (2008) 3240-3246.
[39] Y. Dou, R.G. Egdell, T. Walker, D.S.L. Law, G. Beamson, N-type doping in CdO ceramics a study by EELS and photoemission spectroscopy, Surf. Sci. 398 (1998) 241-258.
[40] A. Anders, G.Y. Yushkov, Ion flux from vacuum arc cathode spots in the absence and presence of a magnetic field, J. Appl. Phys. 91 (2002) 4824-4832.
[41] E. Byon, A. Anders, Ion energy distribution functions of vacuum arc plasmas, J. Appl. Phys. 93 (2003) 1899-1906.
[42] A. Anders, Atomic scale heating in cathodic arc plasma deposition, Appl. Phys. Lett. 80 (2002) 1100-1102.
[43] A. Segura, J.F. Sanchez-Royo, B. Garcia-Domene, G. Almonacid, Current underestimation of the optical gap and Burstein-Moss shift in CdO thin films: A consequence of extended misuse of α2-versus-hν plots, Appl. Phys. Lett. 99 (2011) 151907-1-151907-3.
[44] E. Martin, M. Yan, M. Lane, J. Ireland, C. Kannewurf, R. Chang, Properties of multilayer transparent conducting oxide films, Thin solid films 461 (2004) 309-315.

Table 1 Properties of ICO films with different In concentrations.

In (at. %)	**$I_{(200)}/I_{(220)}$**	**D (nm)**	**RS (Ω/□)**	**E_g (eV)**	**λ_{RT} (nm)**
0%	0.43	40	19±1	2.67	
1.2%	0.50	44	4.4±0.1	2.98	2188
2.2%	0.55	42	3.7±0.2	3.01	1915
2.4%	0.77	43	3.4±0.2	3.07	1734
4.2%	3.06	43	3.1±0.1	3.11	1603
9.1%	3.15	35	3.8±0.2	3.28	1413

Table 2 Comparison of electrical properties of ICO thin films prepared by various techniques. Mobility (μ)×cm^2/Vs, resistivity (ρ)×10^{-5} Ωcm, carrier concentration (n)×10^{20} cm^{-3}

In(at. %)	Technique	d (nm)	μ	ρ	n	Substrate	Reference
1.2	PFCAD	230	142	9.9	4.5	Glass	This work
2.2	PFCAD	220	125	7.9	6.3	Glass	This work
2.4	PFCAD	220	120	7.6	6.9	Glass	This work
4.2	PFCAD	240	104	7.2	8.3	Glass	This work
9.1	PFCAD	260	66	8.7	10.8	Glass	This work
0.5	PLD	150	264	3.2	7.5	MgO (001)	[43]
2	PLD	100	155	2.9	14.1	Quartz	[19]
3.8	PLD		96.2	6	10.9	Glass	[13]
2.6	MOCVD	200	120	5	14	MgO (100)	[30, 36]
4.3	MOCVD	200	≈75	9.6	8.6	Glass	[30, 36]
5	MOCVD	150	69	6	15.1	Glass	[12]
5	Sol-gel	100-250	≈32	60	2.8	Glass	[14]
5.9	Spray Pyrolysis	450	34	45	3.7	Glass	[10]
$CdIn_2O_4$	PLD	<150	19.1	115	2.8	MgO (111)	[44]
$CdIn_2O_4$	MS		23	120	2.3	Glass	[33]
$CdIn_2O_4$	MS	290	44.2	23	6.1	Glass	[34]
$CdIn_2O_4$	MS	300-600	54	2.3	7.5	Glass	[35]

Figure captions

Fig.1. SEM images of ICO thin films prepared at 220 ℃ and 7mTorr (a) undoped, inset: higher resolution image (100 nm), (b) 9.1 at. %.

Fig. 2. AFM morphologies of the ICO thin films with different In concentrations prepared at 220 ℃ and 7 mTorr (a) 0%, (b) 1.2%, (c) 2.2%, (d) 2.4%, (e) 4.2%, (f) 9.1%.

Fig. 3. XRD patterns of ICO thin films with different In concentrations prepared at 220 ℃ and 7mTorr.

Fig. 4. Electrical properties of the ICO thin films with different In concentrations prepared at 220 ℃ and 7mTorr.

Fig. 5. Optical transmittance and reflectance of the ICO/glass stacks with different In concentrations. The glass substrate is 1 mm thick. The AM1.5 solar spectrum is shown for comparison. a-undoped, b-1.2%, c-2.2%, d-2.4%, e-4.2%, f-9.1%.

Fig. 6. Optical bandgap of the ICO thin films with different In concentrations prepared at 220 ℃ and 7mTorr. (a) Tauc plot for direct bandgap, (b) bandgap vs In concentration.

Fig. 7. Optical bandgap of the doped CdO thin films as a function of two-thirds power of the carrier concentration ($n_e^{2/3}$).

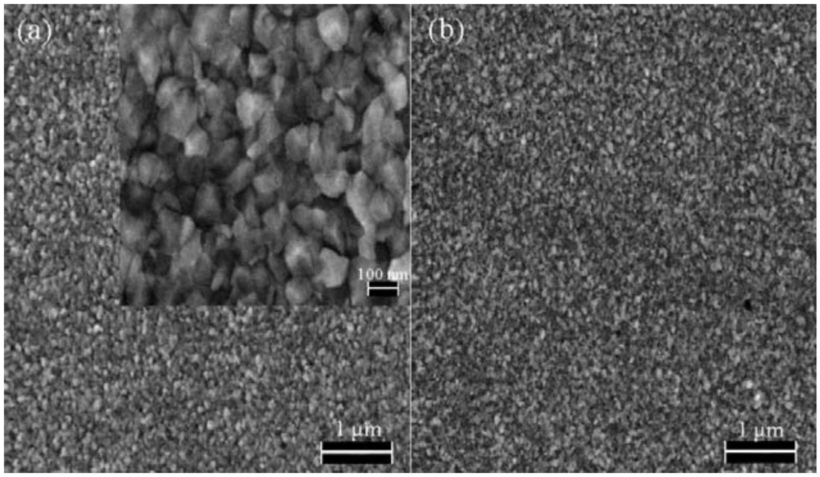

Fig. 1

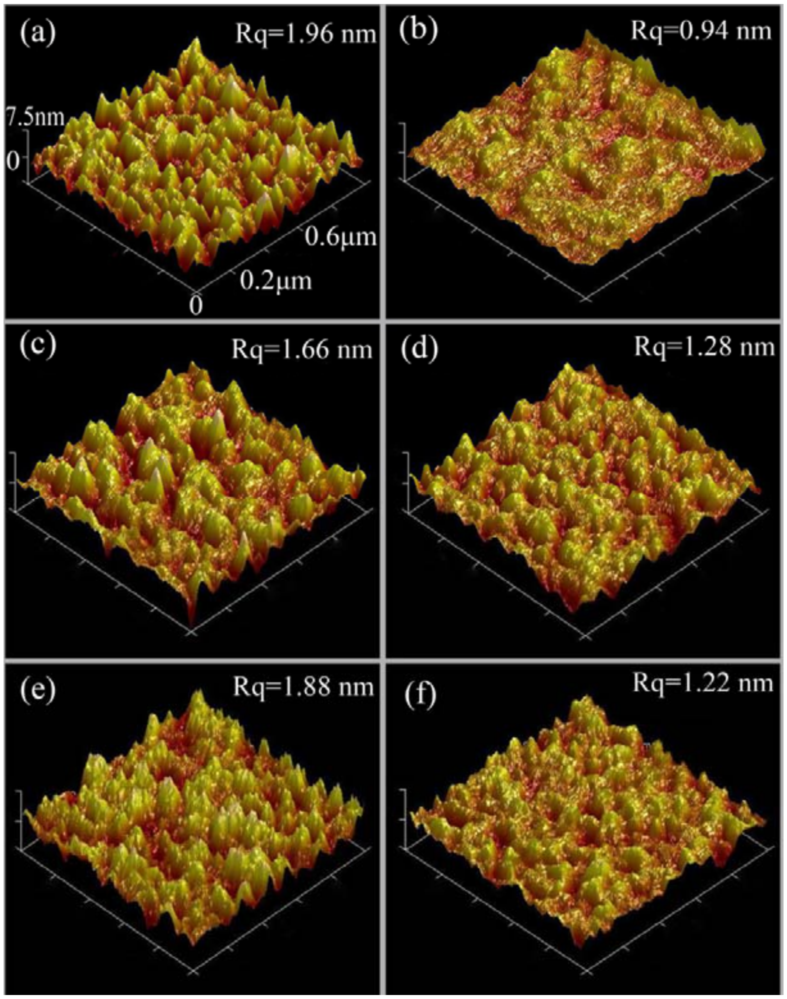
(a)
Rq=1.96 nm
7.5nm
0
0.6μm
0.2μm
0
(b)
Rq=0.94 nm
(c)
Rq=1.66 nm
(d)
Rq=1.28 nm
(e)
Rq=1.88 nm
(f)
Rq=1.22 nm

Fig. 2

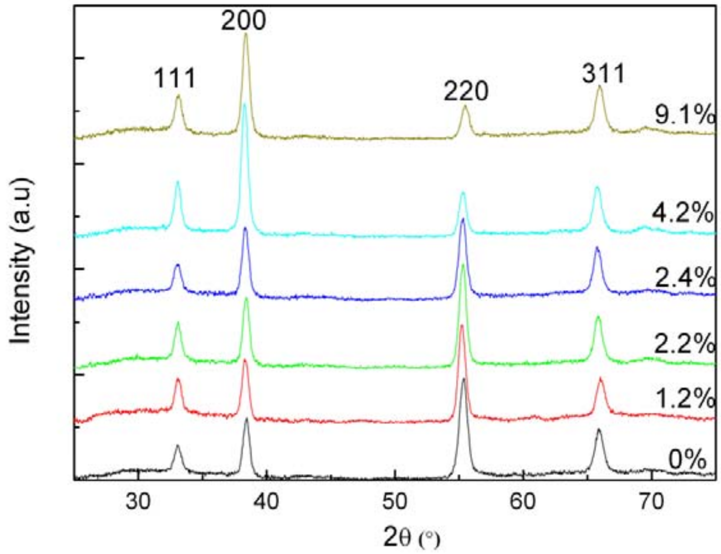

Fig. 3

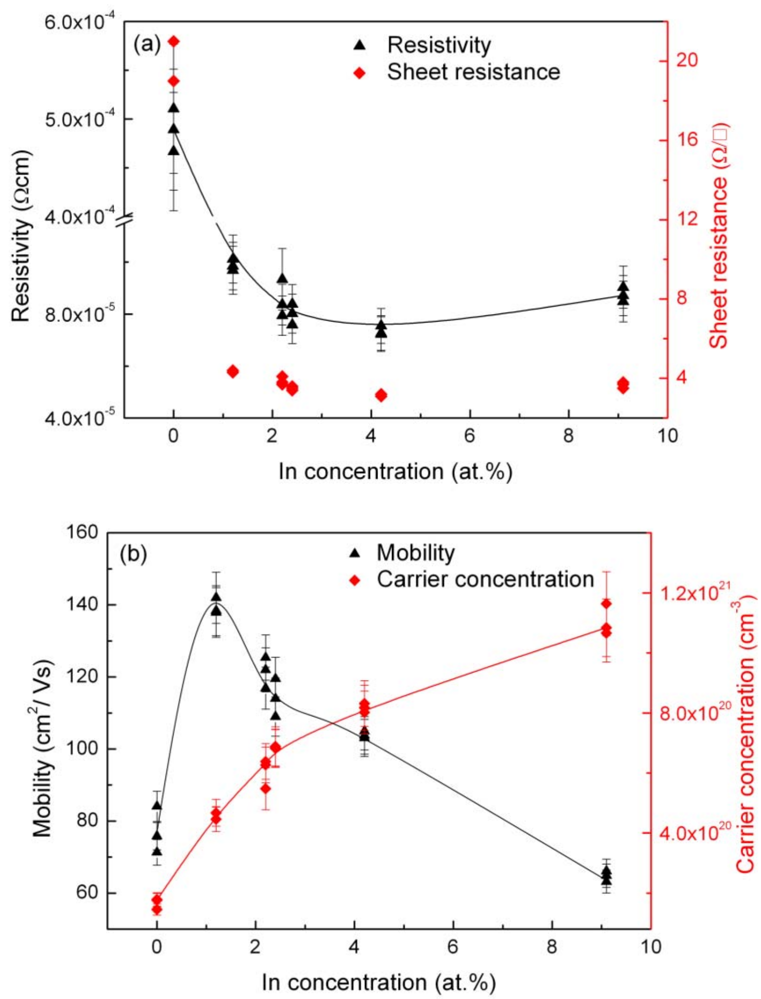

(a)
Resistivity
Sheet resistance
Resistivity (Ωcm)
Sheet resistance (Ω/□)
6.0x10^-4
5.0x10^-4
4.0x10^-4
8.0x10^-5
4.0x10^-5
20
16
12
8
4
0
2
4
6
8
10
In concentration (at.%)
(b)
Mobility
Carrier concentration
Mobility (cm^2/ Vs)
Carrier concentration (cm^-3)
160
140
120
100
80
60
1.2x10^21
8.0x10^20
4.0x10^20
0
2
4
6
8
10
In concentration (at.%)

Fig. 4

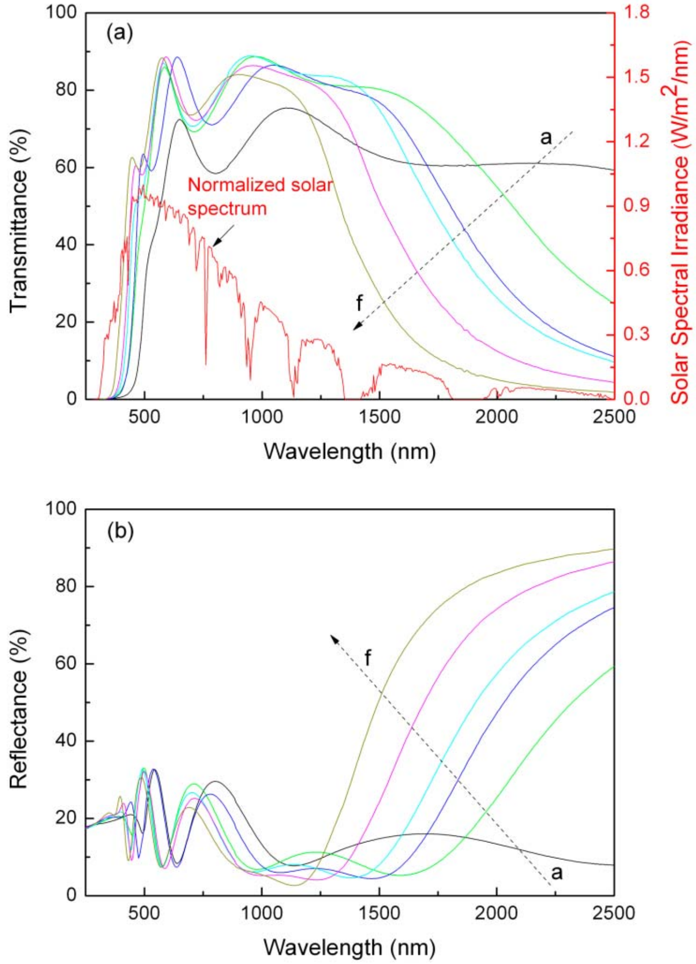
(a)
Transmittance (%)
Solar Spectral Irradiance (W/m^2/nm)
Normalized solar spectrum
a
f
Wavelength (nm)
(b)
Reflectance (%)
f
a
Wavelength (nm)

Fig. 5

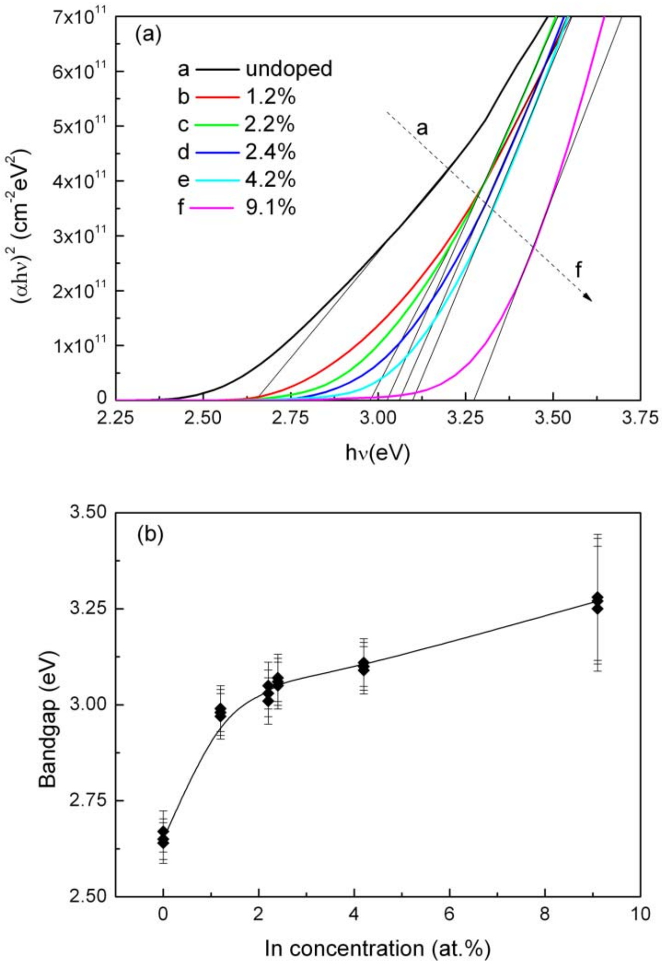
(a)
a undoped
b 1.2%
c 2.2%
d 2.4%
e 4.2%
f 9.1%
a
f
$(\alpha h\nu)^2$ ($cm^{-2}eV^2$)
hν(eV)
(b)
Bandgap (eV)
In concentration (at.%)

Fig. 6

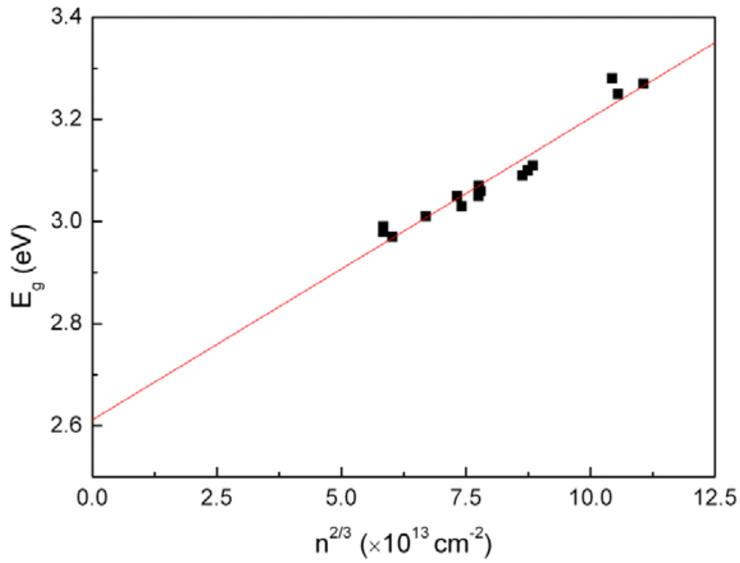

Fig. 7